Precise Measurement of the Electron Beam Current Measurement in a TEM

Florian F. Krause[a,1,*], Marco Schowalter[a,1], Oliver Oppermann[a], Dennis Marquardt[a], Knut Müller-Caspary[a], Robert Ritz[b], Martin Simson[b], Martin Huth[b], Heike Soltau[b], Andreas Rosenauer[a]

[a] *Institut für Festkörperphysik, Universität Bremen, Otto-Hahn-Allee 1, 28359 Bremen, Germany*
[b] *PNSensor GmbH, Römerstraße 28, 80803 München, Germany*

Abstract

Modern quantitative TEM methods such as the ζ-factor technique require precise knowledge of the electron beam current. To this end, a macroscopic Faraday cup was designed and constructed. It can replace the viewing screen in the projection chamber of a TEM and guarantees highly accurate measurement of the electron beam with precision only limited by the used amperemeter. The easy to install, affordable device is shown to be highly apt for precision measurement of currents $> 5\,\mathrm{pA}$. The Faraday cup results are used for an assessment and a comparison of various other beam current measurement methods. It is found that the built-in screen amperemter of the used TEM is quite inaccurate and that measurements using the screen in general tend to underestimate the current. If present, the drift tube of a spectrometer can also be used as a Faraday cup, but certain described peculiarities have to be taken into account. Direct ultrafast electron detection cameras allow precise measurement at very small currents. For the electron counting technique, which exploits single electron detection capabilities of STEM detectors, a systematic current underestimation was observed and investigated. This results in a reformulated routine for the method and with these improvements it is demonstrated to be capable of accurate high-precision measurements for currents $< 5\,\mathrm{pA}$.

Keywords: Current measurement, TEM, quantitative STEM, HAADS, Faraday cup, zeta factor, accidental electrons

1. Introduction

Quantitative scanning transmission electron microscopy (STEM) has become one of the standard tools for structural and compositional investigations in electron microscopy. Its robust high-resolution and intuitive interpretation with various detectors makes it very versatile. While electron detectors allow for the detection of elastically and quasi-elastically scattered electrons, energy-dispersive X-ray (EDX) detectors or electron energy-loss spectrometers (EELS) give access to inelastic processes. These and and their combination yield multidimensional datasets, which can be used to determine many specimen properties simultaneously at atomic resolution [1**?** –3].

For the quantitative interpretation and evaluation of experimental STEM data it is usually necessary to normalise the measurements in regard to the electron dose used for each data point. For some methodologies such as quantitative high-angle annular darkfield (HAADF) STEM or EDX quantification using the Cliff-Lorimer method a normalisation relative to the incident dose or current can suffice [4–6].

More sophisticated methods however require the precise and accurate knowledge of the absolute electron beam current during the experiment. One example is the ζ-factor scheme for evaluation of elemental concentrations with EDX [7, 8], which has a central role in EDX tomography [9, 10]. Here, concentrations C can be calculated from corresponding EDX intensities A with a proportionality relation

$$C \propto \zeta \frac{A}{D} \tag{1}$$

with the eponymous ζ-factor ζ and electron dose D. Both the precision and the accuracy of the resulting concentrations therefore directly rely on a precise and accurate knowledge of the dose and thus the electron current I. Furthermore, the necessary initial determination of the ζ-factor itself also depends crucially on a current measurement. Even for techniques that do not strictly require it, knowing the absolute dose can yield additional insight in the measurements precision or possible beam damages [11, 12].

The task of measuring the beam current, i.e. the current of the incident beam on the specimen surface itself is thus becoming more and more important. It may sound simple at first – after all, amperemeters with sub-picoampere precision are available – and indeed the emission current of the electron gun is usually accurately measured. But most of the emitted electrons are absorbed by succeeding apertures. This causes drain currents that are oftentimes not measured and reduce the current actually impinging on the specimen by orders of magnitude. The current hence has

*Corresponding author. Tel.: +49 421 216 62266
Email address: f.krause@ifp.uni-bremen.de (Florian F. Krause)

[1] M. Schowalter and F. Krause contributed equally to this work and hence share first authorship.

to be measured in or behind the specimen plane. However, modern transmission electron microscopes use voltages in the 100 kV-range, which means that electrons have enough energy to escape metal surfaces by backscattering or create secondary electrons that do so. Measurements using the viewing screen as implemented in most commercially available instruments can therefore significantly underestimate the actual current.

Several methods of STEM current measurement have been proposed, one of which by authors of this article is employing the single-electron sensibility of HAADF detectors and referred to as »electron-counting« [13]. The objective of this work is a concise comparison of these techniques with respect to their accuracy and precision. These tasks require very reliable reference measurements of the beam current. To this end a macroscopic Faraday cup was constructed and installed in the projection chamber of a microscope. It can guaranty an accurate, lossless detection of the complete beam current. Furthermore, causes for an observed systematic current underestimation of electron counting results are investigated and discussed. A solution in form of a robust procedure for the correction of this error is presented.

2. Current Measurement Techniques

The easiest way of measuring the beam current is using the amperemeter that is connected to the fluorescent screen that is built into most modern microscopes. However, as mentioned in Section 1, the high electron energy can allow an unknown amount of electrons to escape and the current to be underestimated [14].

A robust, proven technical solution for this is a so-called Faraday cup, a vessel which captures the escaping electrons by its geometry. One realisation for this in the TEM context is available in specialised specimen holders that have a miniature cup near the specimen cradle, sometimes referred to as »Faraday cup holders« [15]. However, such holders are quite rare and a comparably expensive solution for the problem. The cup also has to be very small due to the port's and pole pieces' constraints. Therefore a loss of electrons cannot be fully excluded. Additionally, they require to shift the field of view away from the sample, which can make their use excessively tedious in experiments that require a frequent current measurement while a specimen is investigated.

Several other methods have been documented in literature. In the following the ones that will be investigated in this article are concisely introduced.

2.1. From Spectrometer Drift Tube

In microscopes equipped with an energy filter or spectrometer, in which the electron beam is deflected by a magnetic prism, the tube inside this prism can be used as a makeshift Faraday cup [13, 14, 16]: By significantly detuning the prism, all entering electrons are expected to hit the tube wall. Because the tube is curved and several centimeters long, it is also expected that no electrons will be able to escape. Therefore the measured drain current should be equal to the actual beam current.

In the present case the drift tube of a Gatan imaging filter (GIF) was used. Here, the drain current can be tapped by grounding the »drift tube« connector through an amperemeter. Newer models of the GIF even have a built-in amperemeter. The detuning of the prism can then be measured by the energy-loss setting in the filtering software.

2.2. Direct Detection Camera

Another possibility for precise current measurement is the use of a camera with a quantum efficiency suitable for single electron detection. This is found in modern scintillator-free direct detection devices. In the present work a pnCCD was used. The electron beam is spread onto the camera chip and recorded at the highest available frame rate. The singular impinging electrons can be identified in each frame, if the current is small enough. In principle, the detected events can then be counted yielding the number of electrons per frame time and hence the current. In practise, events of multiple electrons impinging simultaneously at the same position will occur for the currents of interest. Therefore the intensity of each event has to be considered. For details of this method the reader is referred to Ref. [17].

2.3. Electron Counting in Detector Scans

Almost every microscope capable of STEM is equipped with a detector based on a scintillator coupled to a photomultiplier tube. In most cases it is designed for HAADF measurements. This kind of detector is capable of registering single impinging electrons [18] and has a linear dynamic range up to the currents of interest here.

Exploiting this capabilities, authors of this paper proposed a method for STEM current measurement, which will be referred to as »electron counting« in the following. For details of the originally proposed procedure, the reader is referred to Ref. [13]. The central idea is to acquire two images without a specimen present in the beam: First, the full beam is focussed on the detector and scanned over it, resulting in a so-called detector scan. From this, the intensity of the full beam J_1 can be determined by averaging over the detector area. A possible intensity offset J_0 can be be calculated from the beam positions besides the detector. Second, STEM images with a very small fraction of the beam are acquired. For this it was proposed to take vacuum scans, i.e. HAADF STEM micrographs of plain vacuum, where absolutely no scattering is expected and making use of the unavoidably occurring accidental electrons that will be detected anyway. Analysing the intensity distribution in histograms of the latter allows for calculating the average intensity caused by a single

electron J_{1e}. The number of electrons n_e in the full beam can then be calculated by a simple division:

$$n_e = \frac{J_1 - J_0}{J_{1e} - J_0}. \tag{2}$$

If the dwell time is known, the current can be calculated from it.

In Ref. [19], Sang et al. proposed a variation, where instead of a vacuum scan they strongly reduce the extraction voltage of the electron gun and scan the focussed beam over a small area of the detector. This removes artefacts from detector inhomogeneities. In a detailed analysis of these low-intensity images, they also found peculiarities in the intensity distribution that are discussed closer in Section 6.

2.4. Signal-to-Noise Ratio in Detector Scans

Another method also based on detector scans was proposed in Ref. [20] based on calculations in Ref. [21]: The ideal signal-to-noise ratio (SNR) of the incoming electron beam is solely given by the Poisson statistics of its shot noise and for a beam with an average of n_e electrons during the dwell time it is given by

$$\mathrm{SNR}_{\mathrm{ideal}} = \sqrt{n_e}. \tag{3}$$

Furthermore with relatively weak assumptions, which apply for scintillator-photomultiplier based detectors, it can be shown that the SNR of the measured signal is given by

$$\mathrm{SNR} = \sqrt{\frac{n_{\mathrm{PMT}}}{n_{\mathrm{PMT}}+1}}\mathrm{SNR}_{\mathrm{ideal}} = \sqrt{\frac{n_{\mathrm{PMT}} n_e}{n_{\mathrm{PMT}}+1}}, \tag{4}$$

where n_{PMT} is the average number of charges that one single beam electron causes at the end of the photomultiplier cascade. n_{PMT} is an absolute measure of the detector sensitivity, but generally not known a priori.

Now the inhomogeneity of the sensitivity of most detectors is exploited. If the detector has at least two areas A and B with different sensitivities, they will have different $n^{\mathrm{A}}_{\mathrm{PMT}}$ and $n^{\mathrm{B}}_{\mathrm{PMT}}$, whereas the beam current and thereby n_e is the same in both areas. With this, from Eq. (4) follows

$$n^{\mathrm{A}}_{\mathrm{PMT}} = \frac{\frac{J_{1\mathrm{A}}-J_0}{J_{1\mathrm{B}}-J_0} - \frac{\mathrm{SNR}^2_{\mathrm{A}}}{\mathrm{SNR}^2_{\mathrm{B}}}}{\frac{\mathrm{SNR}^2_{\mathrm{A}}}{\mathrm{SNR}^2_{\mathrm{B}}} - 1}. \tag{5}$$

All quantities on the right hand side of Eq. (5) can be determined from a detector scan with an inhomogeneous sensitivity. Solving Eq. (4) for n_e finally gives the actual number of electrons and thereby the current, if the dwell-time is known. The precision can be assessed by using more than two regions of the detector.

This method employs similar experimental data as electron counting, but has the advantage, that sensitivity inhomogeneity is inherently considered and the signal of a single electron does not have to be determined.

3. Macroscopic Faraday-cup for Reference Measurements

Because all techniques described in Section 2 have their peculiarities and shortcomings, which are to be investigated in this work, accurate reference measurements are needed. Therefor a dedicated macroscopic Faraday cup was constructed with the primary design focus on guaranteeing that no beam electrons can escape. Opposed to Faraday cup holders, which can suffer from their geometric constraints, this cup was thus built for installation in the projection chamber, where the space allows for a larger device. It was designed as a replacement of the large viewing screen.

The schematic construction is shown in Fig. 1: The cup itself is built from a hollow steel sphere with a thread hole, into which a hollow screw is inserted. The diameter of the sphere is 50 mm. The screw is 25 mm long and the diameter of its bore is of 3.5 mm. The sphere is fixed with the screw below an aluminum plate, whose geometry was chosen to fit the viewing screen space. Employing two Teflon washers, the cup is electrically fully insulated from the plate. The plate is then inserted into the projection chamber and installed in place of the large viewing screen. Thereby it is also grounded, insuring that no unwanted charging occurs. Using the feed-through of the microscope, the sphere is connected to an amperemeter outside the evacuated instrument. The resistance between the inside of the sphere and the amperemeter input was measured to be $< 10\,\Omega$. The upper Teflon washer and the screw head itself were covered with ZnS-based luminescent paint, which enables focussing and threading of the electron beam by eye. When the construction is inserted, the screw bore axis is along the projection direction. Photographs of the Faraday cup and its installation in the microscope are shown in Fig. 2.

If the electron beam is focused to a diameter of less than 1 mm and centered in the screw bore, it can travel down the bore into the sphere, hitting its inner wall. The electrons cannot penetrate the mm-thick steel shell. Secondary or backscattered electrons unavoidably hit the inside of the sphere again. An escape through the bore is geometrically almost impossible. Additionally it is possible to apply a positive suction voltage of up to 54 V to the cup using a battery stack between amperemeter and ground contact to ensure that secondary electrons definitely cannot escape. However, application of this voltage showed no influence on the results with the Faraday cup in any of our investigations and is hence apparently not necessary for this geometry.

Consequently all beam electrons flow through the cable, over the amperemeter to the ground contact, where therefore the entire beam current can be accurately measured. The resistance added by the cup, the cable and the amperemeter is only of few ohms, while the resistance between the electron gun and the cup through the vacuum of the column is of the order of 1 TΩ. The resistance added

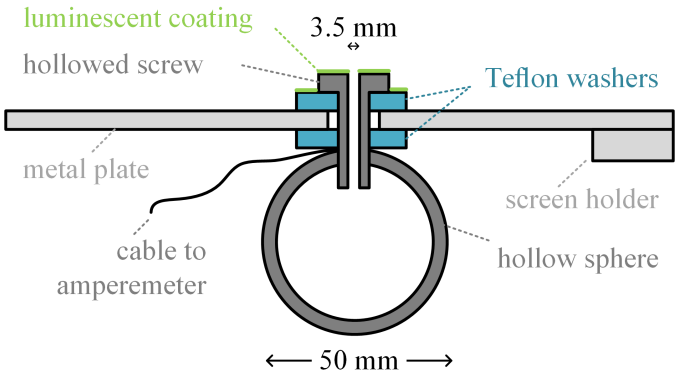

Figure 1: Schematic construction of the Faraday cup: A hollow steel sphere with a diameter of 50 mm is fixed at the bottom of an aluminum plate with a hollowed screw. Screw and sphere are electrically insulated from the plate by Teflon washers. A cable allows to drain current from the sphere. The bore in the screw has a diameter of 3.5 mm. The plate is fixed to the screen holder of the microscope and grounded. Washer and screw head are coated with luminescent paint.

by the measurement equipment hence has no impact on the accuracy.

The geometry of the plate and its fixture to the microscope make it possible to lift the cup like the usual viewing screen. Therefore, lower detectors, cameras and spectrometers can be used as usual. If the cup is installed, the functionality of the microscope is hence not affected except for the big screen not being available. In future designs it is also thinkable to fix the sphere under a viewing screen with a small hole instead of the aluminum plate used here. Measurement routines can thus be conducted as usual with a quick current measurement possible in between, which is another advantage compared to Faraday cups inserted in the specimen holder port.

The complete construction was built for less than 100 EUR, making it very affordable. The installation requires opening the projection chamber, but does not require special tools or knowledge. The exchange from screen to Faraday cup or vice versa takes about one hour, most of which is consumed by the venting and evacuation of the chamber.

In the present case, the Faraday cup was designed for a low-base FEI Titan, but the concept can be adapted to every instrument that has a liftable or retractable screen like the Flucam in high-base Titan microscopes or similar systems of other manufacturers.

4. Details of the experiment

All measurements presented in the following were conducted on a FEI Titan 80/300 G1 microscope equipped with a Schottky field emission gun (FEG), a Fischione Model 3000 HAADF detector and a GIF.

A PNDetector pnCCD was temporarily installed for the measurements discussed in Section 5.3. The camera has a resolution of 264 × 264 pixels and can acquire at a frame time of 0.25 ms if four pixels are binned together.

For the measurement of currents from the Faraday cup and GIF, two Keithley Model 6485 amperemeters were available. All wiring was done with coaxial cables with grounded shielding and BNC connectors. This strongly reduces stray induction effects and allowed an increase of precision with respect to results previously published for the same amperemeter in Ref. [13] by an order of magnitude.

5. Precision and Accuracy of current measurements methods

With the presented Faraday cup installed in the microscope, it was used to analyse applicability of the various methods mentioned in Section 2 in regard to the current measurement in STEM.

5.1. Spectrometer Drift Tube

Even with the low cost and relatively easy installation of the Faraday cup, some will likely hesitate to make alterations to their instrument. Here, the drift tube – if a spectrometer is installed – is a commonly used alternative. Therefore, it was the first subject of the investigation.

The bore into the Faraday cup and the entrance aperture of the GIF were aligned in such a way that a switch between could be done by simply lifting or lowering the cup. The current was measured for different accelerating voltages and spot sizes. For the GIF, the prism excitation was varied i.e. different energy losses were set. Fig. 3 shows the results for exemplary measurements using 300 kV and 80 kV accelerating voltage. If the filter prism is not detuned, relating to zero-loss filtering conditions, no current is measured in the drift tube. This is not surprising; in this case the beam travels though the tube and leaves it at the end without being absorbed. If the prism is detuned, a current is measured, but the result varies strongly with the set excitation not even in a monotonic fashion. For the 300 kV beam, it takes a set energy loss (or gain) of about 9 keV until the measured current stabilises and agrees with the reference result from the Faraday cup. For 80 kV the accurate plateau is reached earlier, but the general observation is the same. Variations of the spot size yield the same curve shapes only with changed amplitudes. The insertion of an energy filter slit in the GIF does not change the behaviour at all.

From this it can be concluded that a GIF drift tube can be a valid Faraday cup for current measurements. However, the amount of prism detuning necessary has to be carefully and thoroughly investigated beforehand. Otherwise the results can be meaningless. The likely reason for the observations is that the mechanics at the end of the drift tube including the filter slit are not electrically connected to the tube. Hence only when the prism excitation is strong enough to push the electrons into the tube wall,

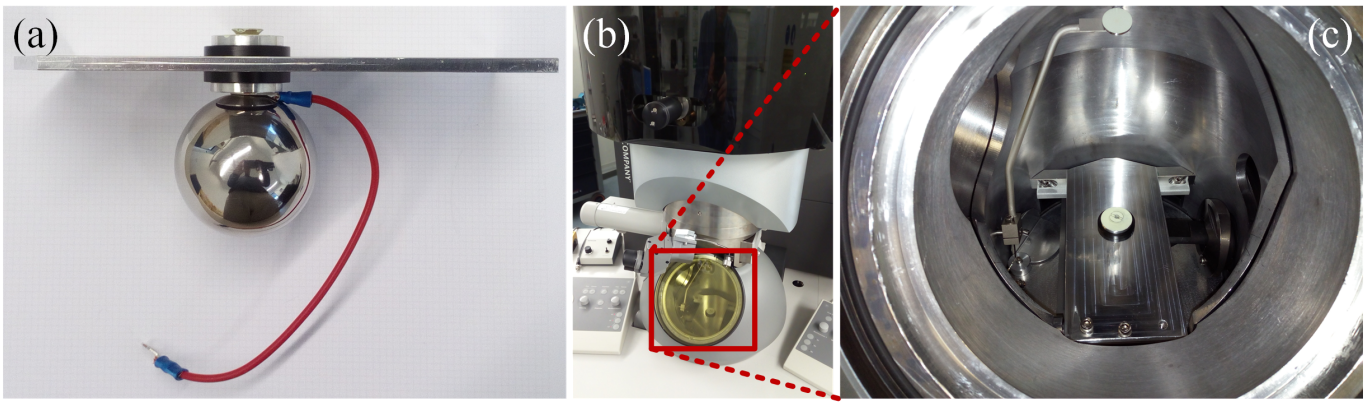

Figure 2: Photographs of the used Faraday cup construction: (a) shows the the baseplate with the sphere mounted below with a hollowed out screw serving as an inlet for the electrons. Sphere and screw are insulated from the plate and connected to a wire that is later used for the current measurement. (b) shows the sphere installed in the FEI Titan 80/300 microscope in place of the large viewing screen.

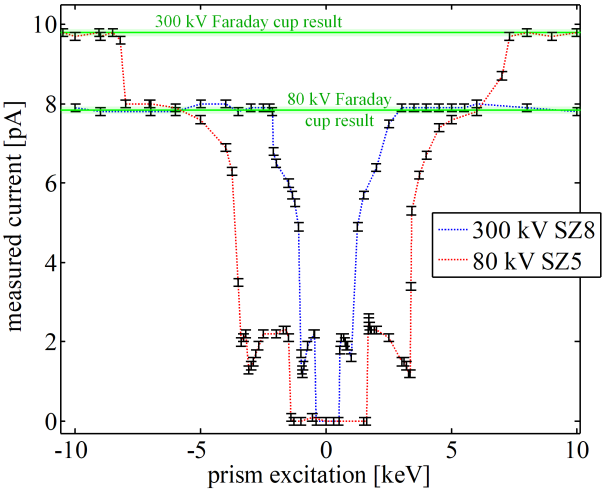

Figure 3: Results of the current measurements using the drift tube of a GIF: The data points connected in blue were measured at 300 kV accelerating voltage and a spot size of 8, the red curve is for 80 kV, spot size 5. The excitation of the filter prism is quantified by the set energy loss. The green lines display the respective reference measurements from the Faraday cup. While the currents from the GIF agree with the reference at very high excitations, intermediate prism settings yield varying and highly inaccurate values.

all of them are captured. As faster electrons are harder to deflect, the necessary prism detuning is larger for the higher acceleration voltage. While these specific results are for a GIF, other filters or spectrometers can be expected to have similar intricacies to be addressed.

Completely switching off the GIF electronics has the same effect as a strong detuning and also yields the correct currents. But of course this has the disadvantage, that it is more difficult to ensure the complete beam entering the filter as no camera behind the filter can be used to image the entrance aperture. Furthermore, if the GIF electronics are not operational, filtering is not possible, excluding a combination of current measurements with energy filtered experiments.

5.2. Built-in Screen

Like most commercially microscopes, the Titan used here is equipped with an internal amperemeter connected to the large viewing screen as the default way for current measurement. As this is the easiest available method for most, it was investigated. The screen current was first measured with the built-in amperemeter, which applies a suction voltage of 24 V. Second, the Keithley amperemeter was used, circumventing the built-in. Here, 54 V suction was applied.

Tab. 1 shows the results for several spot sizes in direct comparison with the Faraday cup results and measurements using the drift tube and very high prism detuning. While the latter agree very well as discussed in Section 5.1, the measurements using the screen show significant inaccuracies: As previously reported [13], the precision of the built-in instrument is limited to $\approx$ 20 pA and therefore it is not usable for smaller currents. But additionally it is apparent that its accuracy is also poor, as it shows deviations also for larger currents.

The measurements with the external amperemeter are more precise and a clear, systematic underestimation can be observed. The currents measured with the flat fluorescence screen are around 5 % smaller than the one observed

Table 1: Current measurement results for a 300 kV beam and different spot sizes from the Faraday cup, the detuned drift tube and the viewing screen: The screen's results show a systematic inaccuracy.

	measured current [pA] from			
spot size	Faraday cup	drift tube	viewing screen	viewing screen (internal amperemeter)
10	2.5 ± 0.1	2.5 ± 0.1	2.1 ± 0.1	-
9	4.5 ± 0.1	4.4 ± 0.1	4.4 ± 0.1	-
8	8.7 ± 0.1	8.7 ± 0.1	8.2 ± 0.1	-
7	17.0 ± 0.1	17.0 ± 0.1	16.6 ± 0.1	-
6	33.6 ± 0.1	33.6 ± 0.1	31.9 ± 0.1	40 ± 20
3	261.0 ± 0.1	261.1 ± 0.1	247.1 ± 0.1	250 ± 20
2	510 ± 0.1	510 ± 0.1	485.3 ± 0.1	450 ± 20

with the cup. As the measurement setup is the same as for the Faraday cup, this has to be attributed to escaping electrons. This is also confirmed by an observed increase in the discrepancy, when the suction voltage is reduced.

As Faraday cup and screen are mutually exclusive, there is a time span between these measurements, in which they are exchanged. However, the results from the GIF stayed the same over this duration and after re-exchange, the Faraday cup result were fully reproduced.

The conclusion to draw from these results is that current measurements via the screen may be be sufficient for exposure time determination or an estimation of possible knock-on damage as they can can give the magnitude of the current, especially if a dedicated amperemeter is used. For more sophisticated applications however, the screen cannot deliver the needed accuracy provided by a Faraday cup.

5.3. Direct Detection Camera

As the shortest frame time of the used pnCCD camera is 0.25 ms and the single electron impacts have to be distinguishable on the frames to be able to count them, the maximum current that can be measured is of $\approx$ 200 fA. As this is an order of magnitude smaller than the currents measured before, the extraction voltage was reduced and the highest spot size 11 was chosen. 2^{18} frames were acquired at frame times of 1, 0.5 and 0.25 ms at a respective binning of 1, 2 and 4 pixels. Fig. 4 shows an exemplary frame and the resulting event statistic. The primary uncertainty in the evaluation is the choice of the thresholds between single and multiple electron events. As displayed in Fig. 4 there are intermediate events that cannot fully be assigned to one distinct electron number. However, as they are more than an order of magnitude less frequent than unambiguously assignable events, the current precision impact of the thresholding choice amounts only to ≈ 2 fA.

The evaluations following Ref. [17] yield a current of 139.5 ± 2.5 fA for a spot size of 11 and 300 kV acceleration voltage. The current measurement with the Faraday cup yields 100 ± 100 fA. This coincides with the pnCCD result, but due to the limits imposed by the amperemeter, the precision is not sufficient for an assessment. Therefore, the

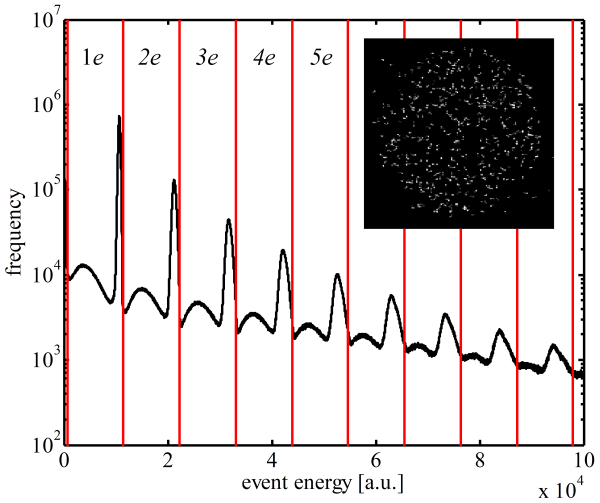

Figure 4: Histogram of the events detected at spot size 11 and 300 kV acceleration voltage on the pnCCD camera: The logarithmic plot shows the frequency of event energies determined from the total intensity of an event. The upper right inset shows an exemplary frame of the measurement. Connected pixels above a certain threshold are counted as a single event. By setting threshold values drawn red in the histogram, the events are assigned different electron numbers. Counting the electrons then allows to calculate the current.

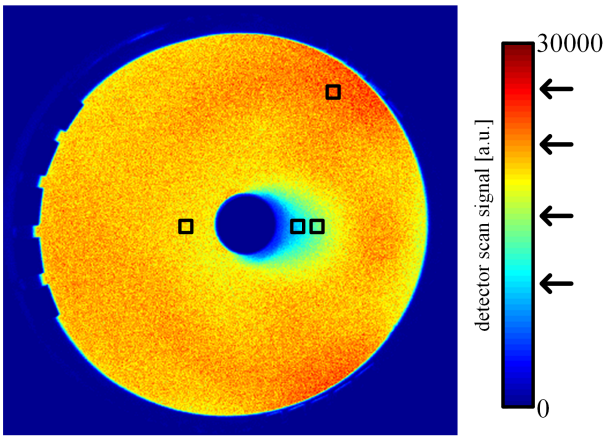

Figure 5: A typical detector scan (4 µs dwell time, spot size 6) as used for the current measurement from the SNR: The signal offset has been subtracted. The four squares mark the regions from which the SNR was determined to calculate the number of electrons. The arrows on the color bar mark the average signal in the respective regions.

electron counting method with the improvements, which will be discussed in detail in Section 6.2, was consulted. It yields 144 ± 7 fA, which is in excellent agreement.

An analogous experiment at 80 kV yielded a current of 234 ± 3 fA with the pnCCD, 200 ± 100 fA from the Faraday cup and 220 ± 25 fA from electron counting.

It has to be concluded, that for small currents, which allow for the distinction of separated events, a direct detection camera can be used for accurate current measurement with exceptional precision.

5.4. SNR analysis

For the current determination from the SNR in different detector regions, detector scans were acquired for several spot sizes and dwell times at 300 kV acceleration voltage. A typical scan is shown in Fig. 5. As the application of Eq. (5) requires the used regions to have distinct SNRs and intensities, only a few regions can be used. In this case four were chosen; they are marked in Fig. 5. Each region contains 169 pixels ensuring a sufficient statistic for the calculation of the SNR, while the sensitivity can be considered constant over the region's extent. Eq. (5) was then solved for all pairwise combinations of these regions.

The values were then averaged and the standard deviation was used as a measure of precision. Dwell times between 2, µs and 4, µs yielded the least variance between different region pairing results. In this way, the results presented in Tab. 2 were gathered from these two dwell times. And while the resulting currents indeed agree with the Faraday cup reference, the precision is not very good: With relative errors above 25 %, the results may be enough for e.g. electron noise estimations, but will not suffice for methods that require precise current measurements such as the ζ-factor method.

Table 2: Current measurement results for a 300 kV beam and different spot sizes from the Faraday cup and the SNR method: The SNR are shown to be accurate, but their uncertainties are rather large.

	measured current [pA] from	
spot size	Faraday cup	SNR analysis
9	3.7 ± 0.1	4 ± 1
8	7.1 ± 0.1	8 ± 3
7	13.3 ± 0.1	19 ± 8
6	25.6 ± 0.1	31 ± 12

Table 3: Current measurement results for a acceleration voltages of 300 kV and different spot sizes from the Faraday cup and the original electron counting method proposed in ref. [13]. The last column shows the relative deviation. A systematic underestimation by the electron counting can be observed.

	measured current [pA] from		
spot size	Faraday cup	electron counting	deviation
10 kV	2.5 ± 0.1	2.2 ± 0.1	12 ± 4 %
9 kV	3.7 ± 0.1	3.2 ± 0.2	14 ± 4 %
8 kV	7.1 ± 0.1	6.3 ± 0.3	11 ± 2 %
7 kV	13.3 ± 0.1	11 ± 1	17 ± 5 %
6 kV	25.6 ± 0.1	22 ± 2	14 ± 7 %

6. Electron Counting for Accurate and Precise Current Measurement

Following the presented analyses, the precision of the electron counting method as laid out in Ref. [13] was also to be examined. However, during this investigation, a systematic inaccuracy was observed: The electron counting result consistently underestimated the reference current from the Faraday cup by 13 ± 1 % as displayed in Tab. 3. Looking closely at the current results presented in Ref. [13], one can already see this inaccuracy masked by the lower precision of the amperemeter there. Thus, an extended study to find possible reasons for this systematic error was conducted.

6.1. Distribution of single event intensities

Of the three values going into the evaluation with Eq. (2), the offset J_0 and the full beam intensity J_1 have relatively clear measurement procedures. While a few minutiae have to be taken into account as was described in Ref. [13], both can be determined quite precisely and therefore be ruled out as causes for the systematic underestimation.

This leaves J_{1e} and thereby $(J_{1e} - J_0)$, the signal caused by a single impinging electron, as the probable culprit. This coincides with an article of Sang et. al, who reported observations that seem to indicate that some electrons may cause significantly reduced signals [19]. Consequently, a strategy similar to the one used there was employed:

Series of vacuum images, i.e. HAADF STEM micrographs without a specimen in the beam path, were taken. The vast majority of these images is plain dark, i.e. the pixels show only the offset intensity J_0 with a certain noise.

But some few pixels show intensities above this noise level. These signal peaks will be called »events« in the following. If the dwell time is below $\approx 2\,\mu s$ the events appear as groups of multiple consecutive pixels above the noise level. This can be attributed to the underlying process having a duration on this time scale. The events were detected by setting a threshold shortly above the noise level and grouping consecutive pixels above it together. The intensity of an event is calculated by summing all pixels belonging to it. If the beam is blanked, there are no events at all. If it is on, they occur at rates of $\approx 1/50\,\mu s$, allowing to detect singular events without significant numbers of double incidences. For a sufficient series size, a comprehensive statistic analysis is possible. An exemplary line of a vacuum image as well as the statistic distribution following from the series is representatively shown in Fig. 6. Multiple series for various dwell times and brightness/contrast settings were acquired, but no significantly different behaviour was found. As J_0 can be determined without problems, it was subtracted from all raw signals, therefore in the following $J_0 = 0$ and hence $J_{1e} = (J_{1e} - J_0)$ is fulfilled. The following investigation hence solely concentrates on the single electron signal.

Looking at Fig. 6, the distribution of events has a distinct Gauss-shaped peak at a finite intensity. The most probable event intensity is found at this peak's position. This intensity coincides fully with the one-electron peak found in the pixel intensity histograms of vacuum images with dwell times above $\approx 4\,\mu s$ as is displayed in Fig. 7 if the different dwell times are considered. This is understandable, as the duration of each event is around $\approx 2\,\mu s$; if the dwell time exceeds this duration, the complete event intensity will be deposited into a single pixel. And this also means, that the position of the Gauss peak in the event statistic can be determined relatively effortless from a single vacuum image without the acquisition of large series and a tedious event thresholding.

However, Fig. 6 also shows a significant amount of events for significantly smaller intensities. Their probability actually appears to increase towards zero. At around twice the threshold, their frequency sharply drops. In Ref. [19], the authors observed a very similar distribution and argued that the difference between threshold and drop off implies that the latter cannot be caused by the former. However, if the event duration is a multiple of the dwell time, the event intensity is spread over multiple pixels and the threshold consequently causes a drop off at a multiple. If the threshold in these investigations is varied, the drop off shifts accordingly. This means, that the drop off observed towards very small event intensities – here and in [19] – has to be considered a measurement artefact. It is unavoidable due to the signal noise, but it seems instructive to extrapolate the event propability towards zero. To this end, a Gauss distribution sitting on an exponential distribution was used as a model and fitted to the measured distribution. The result appears to be a plausible candidate for the real distribution of events.

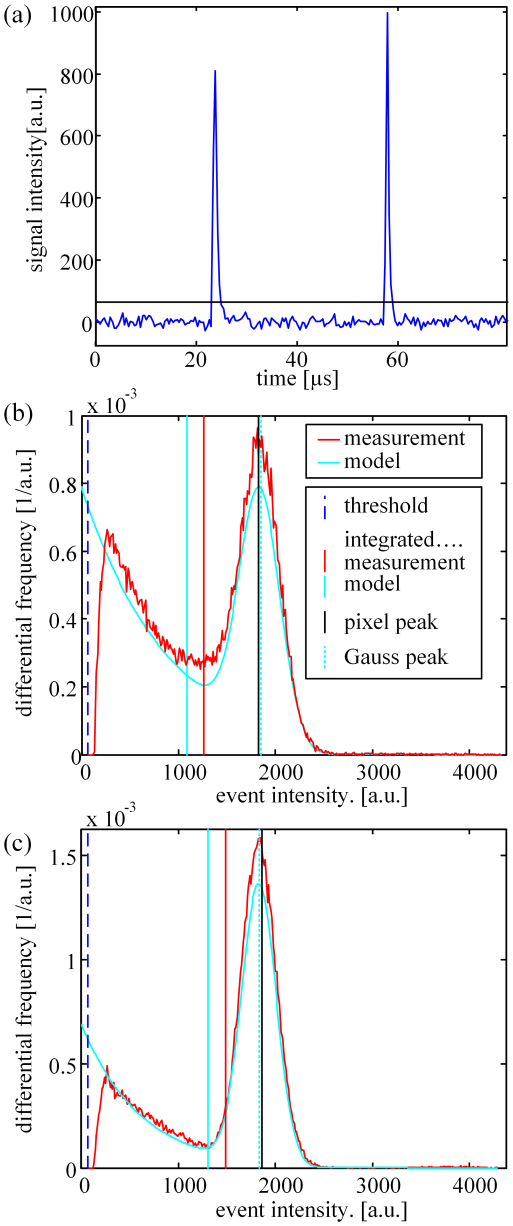

Figure 6: Statistical analysis of events in low-intensity images: (a) shows a typical scan line of a vacuum STEM image. Pixels above the threshold are grouped and added. The result for a dwell time of 0.4 µs is the distribution shown in (b) with the observed frequency of events in red and the model extrapolated to small intensities in cyan. The vertical lines in red and cyan mark the respective expectation values. The black line represents the result of the pixel statistics from Fig. 7. The dotted cyan line marks the maximum of the observed Gaussian maximum. (c) shows the same evaluation for a low-intensity detector scan instead of a vacuum scan with all other parameters held constant. It can be observed that (b) and (c) show very similar characteristics, the only difference being the elevated probability for low-intensity events in (b).

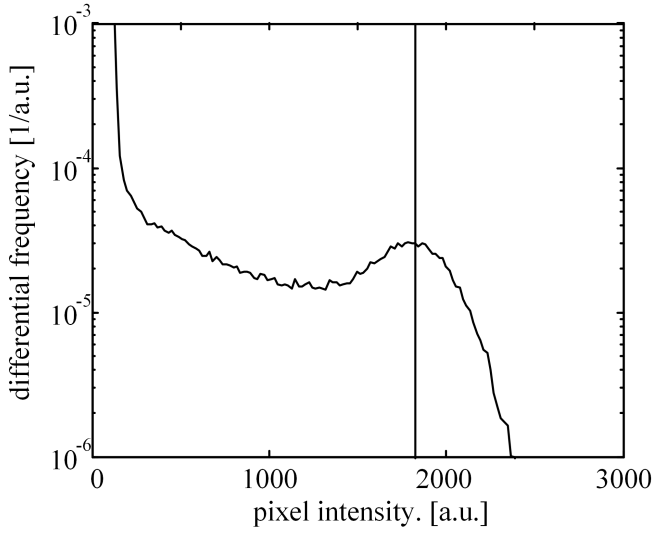

Figure 7: Statistical analysis of the pixel intensities in a vacuum image of 4 µs dwell time (the intensity values have been multiplied by a factor of 10 to account for the different dwell time compared to Fig. 6): While most pixels are dark as seen by the strong frequency increase towards lower intensities, there is also an approximately Gaussian maximum observed at the same intensity that shows the most frequent events in Fig. 6.

Naturally the question, how these low intensity events have to be considered for electron counting, arises. Sang et al. propose the interpretation that these events correspond to beam electrons, which cause a smaller signal. Consequently, one would have to use the expectation value of the whole distribution as J_{1e} instead of the Gauss peak intensity. In the present case, this would amount to a reduction of J_{1e} by $\approx 40\,\%$, if the modelled distribution is used, and by $\approx 30\,\%$, if the measured curve is used. Due to Eq. (2), this would translate into an increase of the current result of the same amount. Notwithstanding the question, whether the modelling of the distribution twowards zero has merit, both increases exceed the observed underestimation by far and would, if applied cause an even worse overestimation.

A possible source of error here could be the use of vacuum images, which entail the complex angular distribution of the accidental electrons and the nonhomogeneity of the detector sensitivity. Furthermore the not fully known origin of the accidentals (some experiments conducted to find out the origin of the accidental electrons are described in appendix Section Appendix C) may also cause a unknown energy distribution of these electrons. To exclude these uncertainties, the above event statistic evaluation was repeated for low-intensity images, where the beam was scanned over a small homogeneous detector area, while the current was drastically reduced by lowering the extraction voltage. The number of events per image was similar to the corresponding vacuum images. The analogous analysis results are also shown in Fig. 6: The qualitative statements made previously also fully apply here: Again an approximately exponential distribution towards small intensities is found and again the artificial drop off can be compensated by a fit. Furthermore, the Gauss peak is found at the exact same position as in the vacuum images and again coincides with the pixel statistic maximum for larger dwell times. The only difference is that low-intensity events are less frequent than before. Nevertheless, the reduction of J_{1e} that would have to follow from it is of $\approx 30\,\%$ with the modelling and $\approx 20\,\%$ without it. The latter is in very good agreement with Ref. [19], but both reductions would reduce the agreement with the Faraday cup result.

What can be drawn from this findings? If the low-intensity events are assumed to be caused by impinging electrons, the corresponding modification to the electron counting would yield currents significantly higher than the Faraday cup references. One interpretation could be the suspicion that the cup measurements have a systematic error, e.g. due to the loss of some beam electrons. But given its geometry and that it has been shown to be very consistent with the various other methods in Section 5 this seems highly unlikely. The investigations in Section 5.4 were done on detector scans acquired in the exact same session as these and even with their limited precision, they indicate strongly, that the amperemeter readout for the Faraday cup cannot be more than 20 % off.

Therefore, the authors of this paper have to conclude, that not all found events are caused by beam electrons. Some appear to be caused by other, secondary processes. Especially the low-intensity events towards zero cannot be completely attributed to single beam electrons. Indirectly, the beam current has to be their origin in some form, because with a blanked beam none are detected. But a significant amount of these events would appear not to be beam electrons directly hitting the detector. Possible other origins are X-rays caused by electrons hitting other surfaces in the projection chamber, which can also produce photons in the detector's scintillator [22]. Secondary charges emerging from electrons impinging on the metal fringe of the detector or other metal components in the chamber may also play a role. An indication towards these effects is the increased probability for low-intensity events in the vacuum scans compared to the images acquired with the reduced beam: For the former a large current of electrons is present in the projection chamber even though it does not hit the detector directly. This can cause the described secondary signals. Others events likely occur from delayed spontaneous signals due to the previous excitation in the PMT, so-called afterpulses [23, 24].

As the events in question seem to occur unavoidable yet are barely above the noise limit and are only fully detected in large statistical investigations, the experimental answer to their origin will be very difficult to give. Changes in the projection chamber such as lifting the Faraday cup or inserting the beam stop have no significant influence on the statistic. For an acceleration voltage of 80 kV the findings can be reproduced.

In the scope of this paper, the authors hence have to confine themselves to the result, that not all low-intensity

events are beam electrons. Yet the underestimation observed, when they are completely ignored, indicates that some are.

6.2. Proposed Procedure for Electron Counting

Despite this lack of a conclusive explanation for the low-intensity events, which may be unsatisfactory from a scientific perspective, from a technical standpoint the observation of the systematic difference between Faraday cup and electron counting result allows for the correction of the electron counting routine: As the counting results have been found to be $13 \pm 2\,\%$ smaller consistently over multiple orders of magnitude of current, for different brightness/contrast settings of the detector and for different acceleration voltages, an empirical gauging factor F can be used. The factor will be individual for different detectors and possibly readout electronics, but after it is determined, it is universal for the specific measurement setting. The factor also has not changed over a time span of two years and thus appears also to be constant.

Incorporating the effects described in Ref. [13] and the peculiarities found and described above, the following procedure is proposed:

0. At the very first measurement, several different currents are measured both directly with an amperemeter and a Faraday cup and with the following steps with a gauging factor set to $F = 1$. In order to achieve comparable precisions, currents between 1 pA and 10 pA are ideal for an amperemeter precision of 0.1 pA. The resulting current values are divided and yield the gauging factor

$$F = \frac{I_{\text{Faraday cup}}}{I_{\text{electron counting with } F=1}}. \tag{6}$$

   If all currents lead to a similar factor, the average of them is the factor used further.
   This only has to executed once. In all further measurements one can start with this F and the following steps
1. The detector's contrast/brightness settings are set to deliver a linear dynamic range up to the full beam intensity.
2. A vacuum image, i.e. a STEM micrograph without a specimen in the beam path, is recorded at a dwell time $t_{\text{vac.im.}}$ above 4 µs (in order to avoid a smearing of events over multiple pixels). In a histogram the one-electron peak intensity J_{1e} is identified.
3. Then, a detector scan is acquired by focussing the beam and scanning it over the detector. Instead of taking one single scan, it is advisable to acquire multiple at a very short dwell time $t_{\text{vac.im.}} \leq 0.5\,\mu\text{s}$ (to avoid artefacts occurring from the full beam resting on the detector for too long [13]). From the average of these scans, an intensity histogram is formed, in which the peak intensities for the offset intensity J_0 and the mean detector intensity J_1 are identified.
4. The current then can be calculated from

$$I_{\text{electron counting}} = F\,\frac{J_1 - J_0}{J_{1e} - J_0}\,\frac{e}{t_{\text{vac.im.}}}. \tag{7}$$

The proposed dwell times and currents are ideal for a Fischione Model 3000 HAADF detector, for other instruments they may have to be adapted slightly.

6.3. Precision and Accuracy of the Proposed Method

To finally asses the quality of the proposed method, Tab. 4 shows the resulting currents for various spot sizes and acceleration voltages in comparison with the Faraday cup and other results. With the applied gauging factor, the electron counting currents are accurate. And for small currents $\lessapprox 2\,\text{pA}$ the results are also more precise than the amperemeter readouts, making it a viable and easily available method for the low-current regime.

For larger currents $\gtrapprox 10\,\text{pA}$, electron counting is likewise accurate, but its precision becomes inferior to the Faraday cup. This is due to the necessity to widen the liner dynamic range for the higher current, which compresses the single electron signal.

7. Summary and conclusions

A macroscopic Faraday cup that can be installed in the projection chamber of a transmission electron microscope was designed, constructed and installed in a FEI Titan microscope. Thanks to its geometry and size, the cup guarantees the registration of all beam electrons and thereby an accurate current measurement, whose precision is only limited by the used amperemeter. It is hence an ideal and affordable addition to the electron microscope, if quantitative methods that require precise current knowledge are to be used. With further future development it would be possible to combine the Faraday cup with the usual screen or flucam, to yield an intuitive, easy to use current measurement instrument to all microscopes

The data acquired with the Faraday cup were used as a reliable reference for the assessment of various further current measurement methods.

The readout from the screen amperemeter of the microscope itself has been shown to be not only imprecise but also inaccurate and unfit for quantitative purposes.

Especially for small currents in the femtoampere range, a direct electron detection camera can yield very precise results.

A method that derives the current from the SNR in detector scans has been shown to work accurately but will be difficult to apply for precise measurements due to a large spread in the evaluation results.

For the technique of electron counting, where the single electron sensitivity of STEM detectors is exploited, a deviation from the other measurement techniques was

Table 4: Current measurement results for a acceleration voltages 300 kV and 80 kV and different spot sizes from the Faraday cup, electron counting and one of the previously described methods if available: The electron counting currents set in bold font were used to determine the gauging factor $F = 1.149$, their agreement with the Faraday cup results is hence by construction. A very good agreement is observed.

	measured current [pA] from		
spot size	Faraday cup	electron counting	other method
11 @ 300 kV (reduced extraction voltage)	0.1 ± 0.1	0.144 ± 0.007	0.140 ± 0.003 (pnCCD)
10 @ 300 kV	2.5 ± 0.1	$\mathbf{2.6 \pm 0.1}$	-
9 @ 300 kV	3.7 ± 0.1	$\mathbf{3.7 \pm 0.2}$	4 ± 1 (SNR)
8 @ 300 kV	7.1 ± 0.1	$\mathbf{7.2 \pm 0.3}$	8 ± 3 (SNR)
7 @ 300 kV	13.3 ± 0.1	13 ± 1	19 ± 8(SNR)
6 @ 300 kV	25.6 ± 0.1	25 ± 2	31 ± 12 (SNR)
11 @ 80 kV (reduced extraction voltage)	0.2 ± 0.1	0.220 ± 0.025	0.234 ± 0.003 (pnCCD)
7 @ 80 kV	3.9 ± 0.1	4.0 ± 0.3	-
6 @ 80 kV	7.9 ± 0.1	8 ± 0.5	-
5 @ 80 kV	15.7 ± 0.1	16.3 ± 1.5	-

observed. Investigations into the origin suggest that secondary electron and X-rays may distort the originally proposed method. A solution for this in form of a gauging factor, which can be determined with the help of the Faraday cup measurements, is suggested. With its employment a new and improved measurement routine for electron counting is suggested that has been shown to be accurate and very precise for smaller currents.

So overall, all investigated current measurement methods, except for the built-in amperemeter of the microscope, were demonstrated to be accurate and in mutual agreement with each other. However, in terms of precision measurements, electron counting is to be preferred for small currents < 5 pA whereas for higher currents Faraday cup measurements with a picoamperemeter are the best choice. In microscopes without spectrometers or in cases, where the spectrometer cannot be switched off or be detuned, the presented design is an affordable, and robust solution.

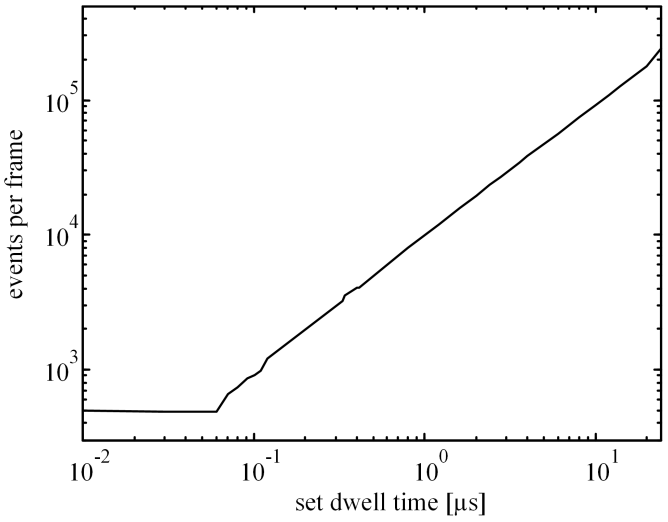

Figure A.1: Number of events detected per STEM image versus the dwelltime set in the microscope software: Below 0.06 µs the event number deviates from the expected linear behaviour and stays constant.

8. Acknowledgments

This work was supported by **deine Projektnummer und eventuell QSTEM2 von Tim**

Appendix A. Irregular Behaviour at Short Dwell Times

During the investigations in Section 6.1, another peculiar behaviour was observed: As the beam current stayed the same for the complete investigation, it is to be expected that the number of electrons and therefore of events per image is proportional to the frame time and thereby the pixel dwell time. For the dwell times used in the investigation in Section 6.1 (> 0.2 µs), this was indeed found to be the case. However, when the dwell times were set up shorter in the microscope software, the number of events per frame behaved as shown in Fig. A.1. While above 0.06 µs the event number shows a strictly linear dependence, all smaller dwell times yield the same unchanged finite number. This has to mean that the effective dwell time, even if set to very small values in the GUI, cannot be decreased below 0.06 µs in the used FEI Titan. This will probably not be critical very often, but if measurements with very short dwell times are conducted on a FEI machine and the exact dwell time is of importance, e.g. in investigations similar to the ones conducted in this paper, one has to be aware of it.

In order to confirm the accuracy of the dwell times used in this paper, the line trigger signal from the microscope was displayed on a Philips 331 combiscope. The time axis was calibrated using a programmable HAMEG HM8122 programmable counter/timer. We found that measured dwell times agree better than 2 % with the dwell time entered in the the microscope software in the range from 0.2 μs up to 4 μs.

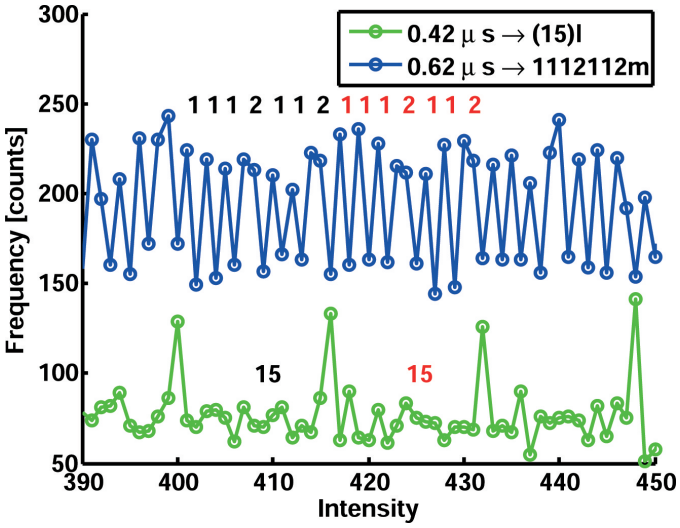

Figure B.2: Comparison of small parts of histograms of vacuum images generated with a bin size of 1 for dwell times of 0.42 μs and 0.62 μs, respectively. Depending on the dwell time certain integer intensity values occur less frequent. The less frequent intensity values do not occur randomly, but exhibit a periodic pattern

Appendix B. Notes on the occurrence of certain integer intensity values

When dealing with histograms the question about a suitable binning arises. Since intensities in the case of our FEI Titan 80/300 ST microscope are 16 bit integers an obvious bin size would be 1 especially for large datasets of about 2k × 2k or 4k × 4k. However, when using this bin size some peculiarities in the frequency of occurrence of certain intensity values were found. Fig. B.2 shows a comparison of small parts of histograms of vacuum images taken at different dwell times. It becomes obvious, that some of the integer intensity values occur less frequent or do not occur at all. The occurrence of less frequent intensity values is not random, but exhibits a periodic pattern. Here we introduce a nomenclature to describe the pattern occurring at the respective dwell time. The nomenclature works as follows: for some dwell times more frequent intensities are interrupted by exactly one less frequent intensity. Then we count the number of consecutive more frequent intensities and note their numbers until the pattern is repeating. This happens after maximum all 16 intensity values. For a dwell time of 0.62 µs a part of a histogram is shown in Fig. B.2. A sequence of 1112112 for the histogram is found. To denote that the sequence is occurring in the more frequent intensity values a "l" is added at the end yielding a descriptor "1112112m" . At other dwell times it can happen that the sequence appears in the less frequent intensities (interrupted by single more frequent intensities). This we denote by adding an "m" at the end of the numerical sequence. For the dwell time of 0.42 μ s (see figure Fig. B.2) a (15)l pattern is observed.

We investigated the patterns for different dwell times as outlined in table Tab. B.1. The patterns are "mirrored" at the dwell time of 0.4 μs. To visualize that, the dwell time and the corresponding pattern (in the above introduced nomenclature) are displayed in an ascending sorting up to 0.4 μs in the left two columns of table Tab. B.1. In the right two columns the dwell time increases from 0.4 μs to 0.79 μs from bottom to top. In fact, beside of exceptions for very low dwell times smaller 0.04 μs the observed patterns are the same for equal distances to the "mirror" dwell time of 0.4 μs. (e.g. the patterns for 0.18 and 0.62 μs are the same and both have a distance of 0.22 μs to 0.4 μs), i.e. the patterns are the same in the left and right column of tableTab. B.1. In a similar manner an "inverting mirror" can be found at 0.2 μs. This not only mirrors, the patterns with respect to the reference dwell time, but also changes an "l" to a "m" or vice versa.

Below 0.4 μs the "less frequent" intensities are even not occurring. The difference between the more frequent occurring intensities and the less frequent intensities becomes small for longer dwell times. The exception for 0.01, 0.02 and 0.03 μs are in line with the observation of the stagnation of the dwell time in Section Appendix A.

The described effect very likely is due to artefacts of the analog to digital converter of the HAADF detector at small dwell times and may lead to difficulties when histograms are used in fitting processes as suggested in reference [**?**] for arbitrary dwell times. However, these difficulties can easily been circumvented by taking the images at multiples of 0.4 μ s dwelltimes. The observed effect might be different for other microscopes and/or ADF detectors.

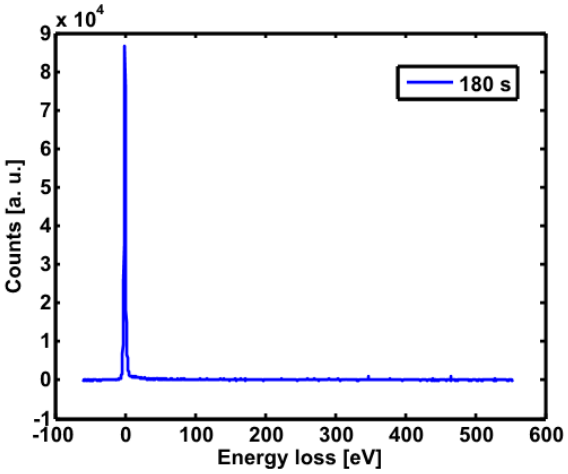

Figure C.3: Low loss EELS spectrum of accidental electrons.

Appendix C. Studies on the origins of accidental electrons

In order to study the origin of the accidental electrons several experiments have been conducted.

First, electron energy loss spectroscopy of the accidental electrons was performed. To do so, the electron

Table B.1: Table of patterns of more or less frequently occurring intensity values for different dwell times in μs.

dwell time	description	dwell time	description
0.01	7l	0.79	smooth
0.02	7l	0.78	(15)l
0.03	7l	0.77	(15)l
0.04	7l	0.76	7l
0.05	7l	0.75	7l
0.06	7l	0.74	7l
0.07	544l	0.73	544l
0.08	544l	0.72	544l
0.09	3l	0.71	3l
0.1	3l	0.70	3l
0.11	3l	0.69	3l
0.12	32222l	0.68	32222
0.13	32222l	0.67	32222
0.14	122l	0.66	122l
0.15	122l	0.65	122l
0.16	122l	0.64	122l
0.17	1112112l	0.63	1112112l
0.18	1112112l	0.62	1112112l
0.19	1m	0.61	1m
0.20	1m	0.60	1m
0.21	1m	0.59	1m
0.22	1112112m	0.58	1112112m
0.23	1112112m	0.57	1112112m
0.24	122m	0.56	122m
0.25	122m	0.55	122m
0.26	122m	0.54	122m
0.27	32222m	0.53	32222m
0.28	32222m	0.52	32222m
0.29	3m	0.51	3m
0.3	3m	0.50	3m
0.31	3m	0.49	3m
0.32	544m	0.48	544m
0.33	544m	0.47	544m
0.34	7m	0.46	7m
0.35	7m	0.45	7m
0.36	7m	0.44	7m
0.37	(15)m	0.43	(15)m
0.38	(15)m	0.42	(15)m
0.39	smooth	0.41	smooth
0.40	smooth		

beam was positioned in a region without specimen and inserted into the GIF. Using the GIF CCD camera the beam was positioned in such a way that the beam could be excluded by the 2 mm or the 1 mm entrance aperture. Since the number of accidental electrons drops with the detection angle [13] the electron beam was just slightly positioned out of the 2 mm aperture. Under this condition EELS spectra were recorded in the low loss region. Figure Fig. C.3 shows a low loss EELS spectrum for an acquisition time of 180 s. Most of the accidental electrons were found to exhibit an nearly vanishing energy loss. The zero loss peak looks slightly asymmetric due to a small additional peak at around 20 eV. This peak is camera length dependent and largest for small camera lengths, but nearly disappearing for camera lengths of around 200 mm. We therefore attribute this peak to be produced within in the projector lens system.

Second, accidental electrons must already exist at the height of the specimen holder: When the beam is scanned on a bar of a Cu grid accidental electrons can still be detected by the HAADF detector. Clearly, the number of accidental electrons is lower in this case since some accidental electrons are blocked by the grid.

Third, residual gas within the column was ruled out by acquiring vacuum images at different pressures at the sample position and counting the number of accidental electrons. Different pressures can be found e.g. directly after inserting the specimen holder without a cooling trap and several hours after inserting the holder and cooling the trap, for which the pressure varied by a factor of 3 . The difference of the number of electrons was found to be only 1.3 %.

References

[1] A. J. D'Alfonso, B. Freitag, D. Klenov, L. J. Allen, Atomic-resolution chemical mapping using energy-dispersive x-ray spectroscopy, Physical Review B 81 (2010) 100101.

[2] G. Van Tendeloo, S. Bals, S. Van Aert, J. Verbeeck, D. Van Dyck, Advanced Electron Microscopy for Advanced Materials, Advanced Materials 24 (2012) 5655–5675.

[3] K. Müller-Caspary, O. Oppermann, T. Grieb, F. F. Krause, A. Rosenauer, M. Schowalter, T. Mehrtens, A. Beyer, K. Volz, P. Potapov, Materials characterisation by angle-resolved scanning transmission electron microscopy, Scientific reports 6 (2016) 37146.

[4] J. M. LeBeau, S. Stemmer, Experimental quantification of annular dark-field images in scanning transmission electron microscopy, Ultramicroscopy 108 (2008) 1653–1658.

[5] A. Rosenauer, K. Gries, K. Müller, A. Pretorius, M. Schowalter, A. Avramescu, K. Engl, S. Lutgen, Measurement of specimen thickness and composition in AlGaN/GaN using high-angle annular dark field images, Ultramicroscopy 109 (2009) 1171–1182.

[6] G. Cliff, G. W. Lorimer, The quantitative analysis of thin specimens, Journal of Microscopy 103 (1975) 203–207.

[7] M. Watanabe, Z. Horita, M. Nemoto, Absorption correction and thickness determination using the zeta factor in quantitative X-ray microanalysis, Ultramicroscopy 65 (1996) 187 – 198.

[8] M. Watanabe, D. B. Williams, The quantitative analysis of thin specimens: a review of progress from the Cliff-Lorimer to the new zeta-factor methods, Journal of Microscopy 221 (2006) 89–109.

[9] D. Zanaga, T. Altantzis, J. Sanctorum, B. Freitag, S. Bals, An alternative approach for zeta-factor measurement using pure element nanoparticles, Ultramicroscopy 164 (2016) 11 – 16.

[10] C. Mahr, P. Kundu, A. Lackmann, D. Zanaga, K. Thiel, M. Schowalter, M. Schwan, S. Bals, A. Wittstock, A. Rosenauer, Quantitative determination of residual silver distribution in nanoporous gold and its influence on structure and catalytic performance, Journal of Catalysis 352 (2017) 52 – 58.

[11] A. De Backer, G. Martinez, K. MacArthur, L. Jones, A. Beche, P. Nellist, S. Van Aert, Dose limited reliability of quantitative annular dark field scanning transmission electron microscopy for nano-particle atom-counting, Ultramicroscopy 151 (2015) 56 – 61. Special Issue: 80th Birthday of Harald Rose; PICO 2015 –

Third Conference on Frontiers of Aberration Corrected Electron Microscopy.
[12] K. Müller-Caspary, F. F. Krause, F. Winkler, A. Beche, J. Verbeeck, S. Van Aert, A. Rosenauer, Comparison of first moment STEM with conventional differential phase contrast and the dependence on electron dose, Ultramicroscopy 203 (2019) 95 – 104.
[13] F. F. Krause, M. Schowalter, T. Grieb, K. Müller-Caspary, T. Mehrtens, A. Rosenauer, Effects of instrument imperfections on quantitative scanning transmission electron microscopy, Ultramicroscopy 161 (2016) 146–160.
[14] D. R. Mitchell, M. J. Nancarrow, Probe current determination in analytical TEM/STEM and its application to the characterization of large area EDS detectors, Microscopy Research and Technique 78 (2015) 886–893.
[15] Double Tilt Analytical Holder Model 646 Datasheet, Gatan Inc., 2018.
[16] R. Rodemeier, personal communication, 2014.
[17] H. Ryll, M. Simson, R. Hartmann, P. Holl, M. Huth, S. Ihle, Y. Kondo, P. Kotula, A. Liebel, K. Müller-Caspary, A. Rosenauer, R. Sagawa, J. Schmidt, H. Soltau, L. Strüder, A pnCCD-based, fast direct single electron imaging camera for TEM and STEM, Journal of Instrumentation 11 (2016) 1–18.
[18] R. Ishikawa, A. R. Lupini, S. D. Findlay, S. J. Pennycook, Quantitative Annular Dark Field Electron Microscopy Using Single Electron Signals, Microscopy and Microanalysis 20 (2014) 99.
[19] X. Sang, J. M. LeBeau, Characterizing the response of a scintillator-based detector to single electrons, Ultramicroscopy 161 (2016) 3 – 9.
[20] B. Haas, Development of quantitative diffraction and imaging based techniques for scanning transmission electron microscopy, Ph.D. thesis, Universite Grenoble Alpes, 2017.
[21] M. Browne, J. Ward, Detectors for stem, and the measurement of their detective quantum efficiency, Ultramicroscopy 7 (1982) 249 – 262.
[22] M. Korzhik, O. Misevich, A. Fyodorov, YAlO3: Ce scintillators: application for X- and soft γ-ray detection, Nuclear Instruments and Methods in Physics Research B 72 (1992) 499–501.
[23] T. Hakamata, Photomultiplier Tubes - Basics and Application, 3 ed., Hamamatsu, Japan, 2007.
[24] U. Akgun, A. Ayan, G. Aydin, F. Duru, J. Olson, Y. Onel, Afterpulse timing and rate investigation of three different Hamamatsu Photomultiplier Tubes, Journal of Instrumentation 3 (2008) T01001.